

Development and simulations of Enhanced Lateral Drift Sensors

A. Velyka,^{a,1} H. Jansen^a

^a*Deutsches Elektronen-Synchrotron DESY,
Notkestraße 85, 22607 Hamburg, Germany*

E-mail: anastasia.velyka@desy.de

ABSTRACT: We present the concept of a new type of silicon tracking sensor called Enhanced Lateral Drift (ELAD) sensor. In ELAD sensors the spatial resolution of the impact position of ionising particles is improved by a dedicated charge sharing mechanism, which is achieved by a non-homogeneous electric field in the lateral direction in the sensor bulk. The non-homogeneous electric field is created by doping implants with a higher concentration with respect to the background concentration of the bulk. A position-dependent charge sharing allows for an improved interpolation of the impact position.

TCAD-based electric field simulations for 2D and 3D geometries as well as transient simulations with a traversing particle for the 2D geometry have been carried out. The electric field profiles have further been optimised for position resolution. The simulations show a strong dependence of the charge sharing mechanism on the deep implant concentration. Optimal values for the deep implant concentration allow for nearly linear charge sharing between two readout electrodes as a function of the impact position. Additionally, the foreseen production technique combining silicon epitaxy and ion beam implantation is outlined.

KEYWORDS: Detector modelling and simulations II, Hybrid detectors, Solid state detectors, Particle tracking detectors (Solid-state detectors), Spatial resolution

¹Corresponding author.

Contents

1	Introduction	1
2	Concept of the ELAD sensor	2
3	TCAD simulations	3
3.1	Electric field	3
3.2	Transients	4
4	ELAD production technique	8
5	Conclusions	8

1 Introduction

Experiments at possible future colliders like CLIC¹ [1] and ILC² [?] aim, among others, for a precise measurement of Higgs decays to pairs of b-quarks, c-quarks and gluons and efficient identification of top quarks in the decay $t \rightarrow Wb$. To this end, the experiments require light-weight detectors with a single-point resolution of a few micrometers. E.g., the tracker and vertex detectors for CLIC require a single point resolution of better than $7 \mu\text{m}$ and $3 \mu\text{m}$, respectively, in the transverse plane to meet the requirements on the track-momentum and impact parameter resolution at a total silicon detector thickness of less than $100 \mu\text{m}$ [2]. Several options for tracking and vertex sensor technology are considered for CLIC, among them are monolithic and hybrid detectors [?].

This work focuses on a new type of a hybrid detector aiming to meet the requirements of the CLIC vertex detector. A common approach to achieve an improved position resolution in silicon detectors is to decrease the readout cell size. This leads to an increased number of readout channels and less area for logic per channel on the readout chip. Additionally, the miniaturisation of interconnection techniques might present limits.

The position resolution can also be improved by means of charge sharing, i.e. by collecting the charge on more than one readout electrode. Geometric charge sharing is used e.g. in the CMS experiment by tilting the sensors in the Endcap [3]. Lorentz drift induced charge sharing by means of a magnetic field is realised in the barrel section of the experiment [?]. However, these two methods do not provide sufficient charge sharing in thin ($\leq 100 \mu\text{m}$) sensors [?], as either unrealistically strong magnetic fields or huge sensor tilts would be necessary, the latter in turn increasing the material budget.

The hybrid detector proposed herein, a so-called Enhanced Lateral Drift (ELAD) sensor in combination with a readout ASIC, introduces a lateral electric field component in the sensor bulk

¹Compact Linear Collider

²International Linear Collider

yielding a lateral charge drift to achieve a position resolution of a few micrometre. This lateral component of the electric field is created by regions deep within the sensor bulk featuring a higher doping concentration with respect to the background doping concentration. This diminishes the need to downsize the sensor pitch while avoiding sensor tilt or magnetic fields.

In Sec. 2, we detail the concept of the ELAD sensor. The SYNOPSYS TCAD simulations and the analysis of charge collection distribution on neighbouring readout electrodes are discussed in Sec. 3. Finally, the production technique is outlined in Sec. 4.

2 Concept of the ELAD sensor

Charged particles traversing a silicon sensor create free electron-hole pairs, which drift inside the sensor and follow electric field lines. In thin standard planar sensors most of the created charge is collected by the nearest electrode and only a small part by the neighbouring electrode. Therefore the position resolution can be improved only by downsizing the distance between strips/pixels, i.e. the pitch size.

The concept of the ELAD sensor relies on charge sharing without the necessity of tilting the sensor or on a magnetic field by means of a modification of the electric field, yielding a position-dependent charge collection by two electrodes [5]. To implement this idea the electric field profile has to be altered. The modified electric field profile is realised by implants with higher doping concentration with respect to the background doping concentration in the bulk. This changes the electric field lines in such a way that the charge carriers move towards the centre between two electrodes, and might diffuse into the next unit cell, leading to a partial collection at both electrodes. The distribution of the collected charge between two electrodes (η -function), where the charge sharing optimises the position resolution, should depend linearly on the MIP position. The ELAD sensor contains two types of deep implants: p-implants and n-implants, in order to reduce the impact of the additional implants on N_{eff} [6]. With such a balancing of p- and n-implants, the same depletion voltage as in a standard planar sensor with an epitaxial layer of the same background concentration and thickness is achieved. The utilisation of two types of deep implants also creates a stronger electric field in the lateral direction, thereby improving the charge-sharing behaviour.

Two types of ELAD sensors are designed – n-in-p (p-ELAD [6]) and p-in-n (n-ELAD) sensors. The p-ELAD sensor represents a p-type sensor with three deep implant layers, each containing one deep n-implant in the middle of the unit cell and one p-implant on each side of the n-implant, three p-type epitaxial layers (needed due to the production process), moderated p-spray isolation, readout implants and electrodes and a backplane implant and electrode. The n-ELAD sensor represents an n-type sensor with three deep implant layers with an inverted doping in each layer with respect to the p-ELAD, three n-type epitaxial layers, readout implants and electrodes and a backplane. The deep p- and n-implants create a local electric field in their vicinity and modify the sensor's electric field profile. The design of the n-ELAD sensor is shown in Fig. 1, where “ro” denotes the readout electrode. The orange (blue) areas represent deep n-implants (p-implants), with a light-green (dark-green) colour showing the epitaxial zone (wafer) of the sensor. The distance from the top of the sensor to the first deep implant layer is 10 μm , the distance between deep implant layers is 10 μm , the total thickness of the epitaxial layer amounts to 30 μm . The pitch for both types of the ELAD is 55 μm in order to match the TimePix3 chip footprint [8].

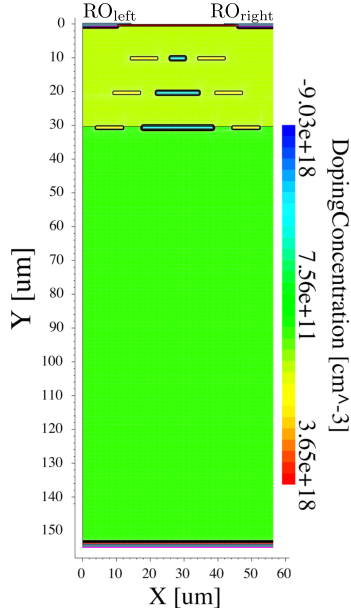


Figure 1: Doping concentration of the n-ELAD sensor.

3 TCAD simulations

The Technology Computer-Aided Design (TCAD) tool by SYNOPSYS was selected as a tool for simulations [7]. Two types of simulations have been performed: electric field simulations and transient simulations with a MIP traversing the sensor. Simulations of the electric field have been performed to describe the behaviour of the ELAD sensors in 2D and 3D. In order to study the performance of ELAD sensors, transient simulations of 2D geometries have been executed for n-type and p-type ELAD sensors. This allows for the analysis of the distribution of the collected charge on neighbouring readout electrodes as a function of the impact position, also known as η -function. The parameters which have been optimised to approach the linear behaviour of the η -function are the distance from the top of the sensor to the first deep implant layer, the distance between deep implant layers, the readout size, the operating voltage and doping concentrations for the deep implants. The profile of the electric field yielding optimal charge sharing is obtained via a scan over the specified parameters. Here, we detail the optimisation process with respect to the deep implant concentration and the readout implant size.

3.1 Electric field

The electric field simulations are performed in a quasi-stationary mode. In this mode the voltage is applied to the contacts of a device. The voltage is ramped to a given value in a number of steps; in each step an electric field profile is calculated. In order to obtain an electric field profile TCAD solves the Poisson's equation with the charge density from the previous iteration as the starting value.

Fig. 2 shows the electric field profile in the lateral direction for a standard planar n-type sensor and the n-ELAD sensor with a total thickness of 150 μm , a thickness of the epitaxial layer of 30 μm and four different deep implant concentrations n_{di} of $2.0 \cdot 10^{15} \text{ cm}^{-3}$, $2.4 \cdot 10^{15} \text{ cm}^{-3}$, $2.8 \cdot 10^{15} \text{ cm}^{-3}$

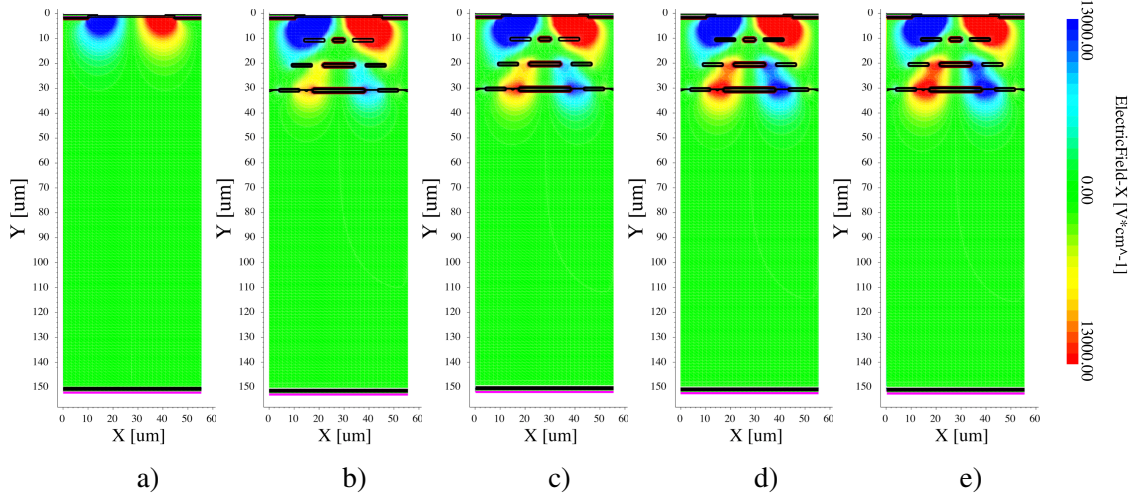


Figure 2: Electric field in the lateral direction for a standard planar n-sensor (a) and the n-ELAD sensors with different deep implant concentrations $n_{di} = 2.0 \cdot 10^{15} \text{ cm}^{-3}$ (b), $2.4 \cdot 10^{15} \text{ cm}^{-3}$ (c), $2.8 \cdot 10^{15} \text{ cm}^{-3}$ (d) and $3.0 \cdot 10^{15} \text{ cm}^{-3}$ (e) at $U = 280 \text{ V}$.

and $3.0 \cdot 10^{15} \text{ cm}^{-3}$. The deep implants create a lateral electric field in the bulk of the sensor. In case of the n-ELAD sensor, the red (blue) areas force holes to move to the right (left) towards the centre between the electrodes. While drifting close to the unit cell border the holes have a sufficiently high probability of diffusing into the next unit cell. Hence, holes are collected by two electrodes. Equivalently, electrons are shared between electrodes in the case of the p-ELAD.

The deep implants create a fixed electric field in the lateral direction. With increasing doping concentration of the deep implants the lateral electric field becomes stronger and its effect on the drift paths of the charge carriers larger. The electric field in the longitudinal direction is created by the applied voltage. The ratio between the longitudinal and lateral components of the electric field changes with the applied voltage and deep implant concentrations. Identification of the optimal operational voltage allows an effective usage of the ELAD sensor.

In Fig. 3 the total electric field with its electric field lines is presented for a standard n-type sensor and the n-ELAD sensor. The electric field lines in the standard planar n-type sensor lead directly to the readout electrodes. In the n-ELAD sensor, the electric field lines change their behaviour with respect to the standard planar sensor, effectively pointing to the centre between two readout electrodes. This renders a position-dependent charge sharing possible.

For the validation of the 2D electric field simulations, the 2D electric fields are compared with the 3D electric fields. Strip and pixel readouts have been realised. In order to optimise the simulation process a quarter of the unit cell has been modeled, since the ELAD design is symmetric. The results of the 3D simulation are shown in Fig. 4. The cross section of the 3D electric field profile resembles the one obtained from the 2D simulations, see Fig. 2 (d).

3.2 Transients

In transient simulations the response of the device to a traversing particle through the device can be simulated. The transient simulation approximates a continuous process as many consecutive

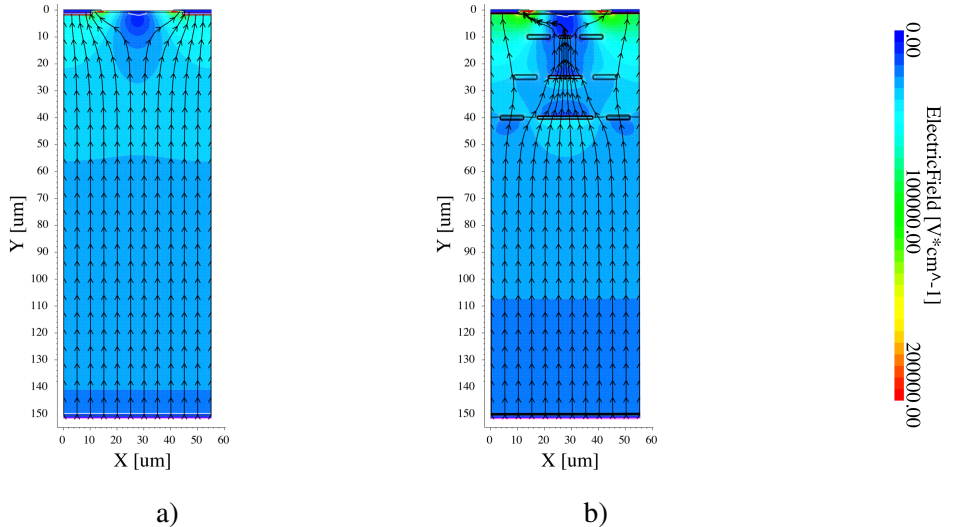


Figure 3: Electric field lines for a standard planar n-type sensor (a) and the n-ELAD sensor with $n_{di} = 2.8 \cdot 10^{15} \text{ cm}^{-3}$ (b) at $U = 280 \text{ V}$.

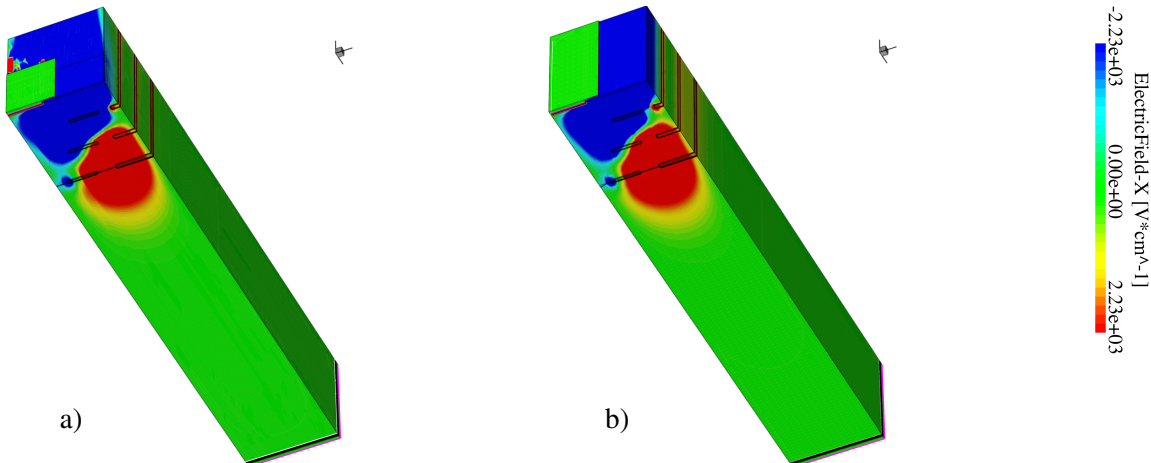


Figure 4: 3D simulation of an electric field in the lateral direction in the n-ELAD sensor with a deep implant concentration $n_{di} = 2.8 \cdot 10^{15} \text{ cm}^{-3}$ with a pixel readout (a) and with a strip readout (b) at $U = 280 \text{ V}$.

frames with a short time difference. In each frame and for each mesh node TCAD solves the Poisson equation and carrier continuity equations for electrons and holes. In order to observe the effect of charge sharing and to avoid the effect of boundary conditions on the edges of the model, a four-unit-cell geometry has been used for the transient simulations. The region of interest extends from the centre of the second readout implant to the next unit cell boundary to the right, which is a half-pitch away. MIP incident positions have been simulated at $0 \mu\text{m}$, $6.3 \mu\text{m}$, $11.6 \mu\text{m}$, $16.9 \mu\text{m}$, $22.2 \mu\text{m}$, $27.5 \mu\text{m}$ from the centre of what is referred to as the left implant.

In Fig. 5 the hole current density in the n-ELAD sensor with $n_{di} = 2.8 \cdot 10^{15} \text{ cm}^{-3}$ for four time steps is shown. In the first two time steps (Fig. 5 (a), (b)) the charge carriers that were created above

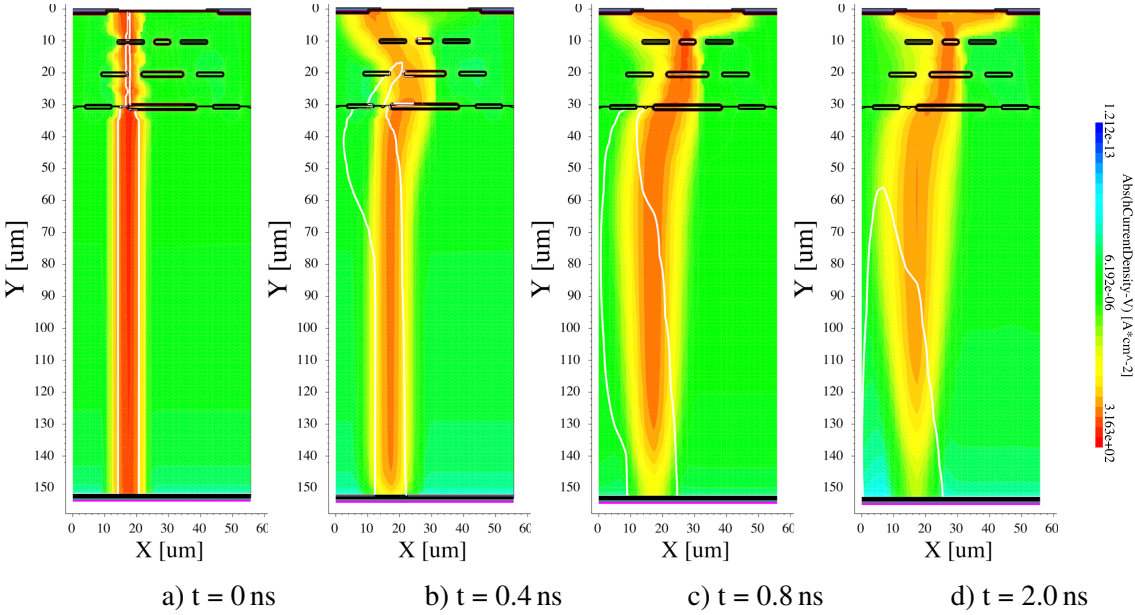


Figure 5: The hole current density for the n-ELAD sensor with $n_{di} = 2.8 \cdot 10^{15} \text{ cm}^{-3}$ is shown at four different points in time for a MIP incident of $16.9 \mu\text{m}$ at $U = 280 \text{ V}$.

the deep implants are collected by the nearest electrode. Charges created beneath the deep implants (Fig. 5 (c), (d)) change their drift path and move to the centre to possibly diffuse into the next unit cell, allowing for charge sharing. Similar results have been produced for the p-ELAD sensor.

In Fig. 6 the collected charge from two neighbouring readout electrodes as a function of the six different MIP positions is presented. The p-ELAD and n-ELAD sensors with different deep implant

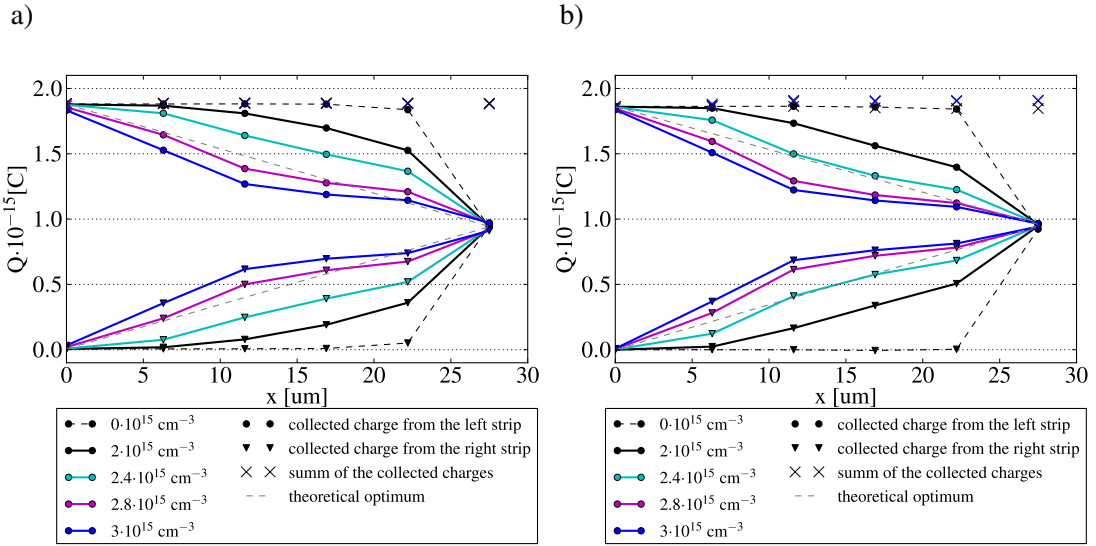


Figure 6: η -function for different deep implant concentrations for the n-ELAD sensor at $U = 280 \text{ V}$ (a) and p-ELAD sensor at $U = 300 \text{ V}$ (b).

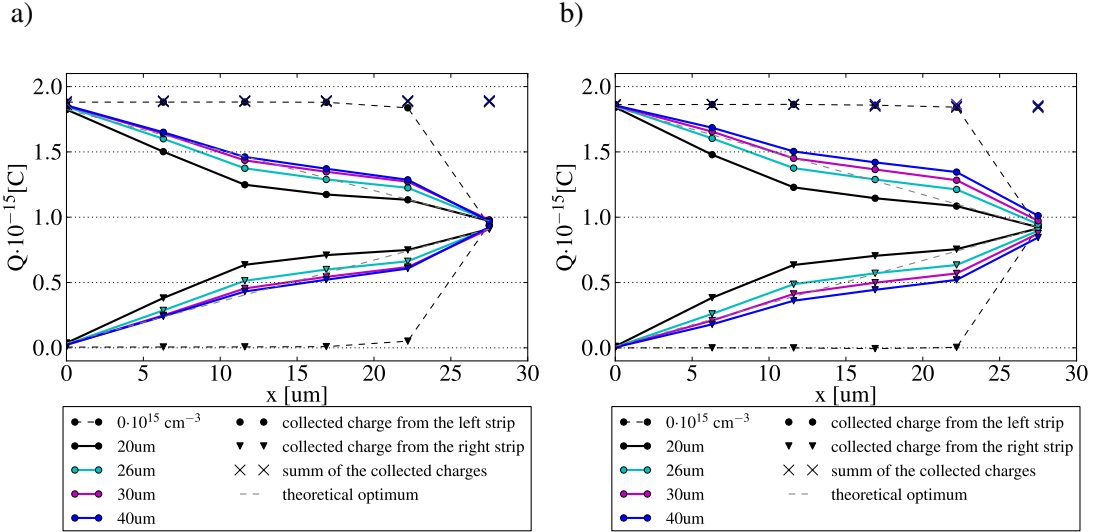


Figure 7: η -function for different sizes of the readout implant for the a) n-ELAD sensor at $U = 275$ V and b) p-ELAD sensor at $U = 300$ V.

concentrations and a sensor with an epitaxial layer without deep implants are shown. The results for the η -function are denoted as follows: circles (triangles) show the collected charge from the left (right) strip, and crosses correspond to the sum of the collected charges. Different deep implant concentrations result in different η -functions (Fig. 6). The lines represent linear extrapolation to guide the eye.

The linearity of the η -functions depends on the deep implant concentration. In the case of the n-ELAD (Fig. 6 (a)) the lowest simulated deep implant concentration of $2.0 \cdot 10^{15} \text{ cm}^{-3}$ (black line) does not yield an optimal change of the η -function profile, but the effect of the deep implants is already noticeable. The blue line shows the result for the highest deep implant concentration, which is equal to $3.0 \cdot 10^{15} \text{ cm}^{-3}$. In this case, the deep implants create an electric field in the lateral direction that is too strong, and the effect of the charge sharing is stronger than at the optimum. For the applied voltage of 280 V the optimal deep implant concentration is $2.8 \cdot 10^{15} \text{ cm}^{-3}$. For the p-ELAD sensor and an applied voltage of 300 V (see Fig. 6 (b)) the optimal deep implant concentration with the most linear η -function profile is $2.4 \cdot 10^{15} \text{ cm}^{-3}$. Hence, for each value of the deep implant concentration an optimal applied voltage exists. The operational voltage should be balanced such that the ratio between the electric field strength in the longitudinal and lateral directions is optimal. If the applied voltage is too low (too high) the effect of the charge sharing by the deep implants is too strong (too weak) resulting in a considerable deviation of the η -function from the linear case.

To study the effect of the readout implant size on the η -function profile several options of the readout implant sizes have been simulated. In Fig. 7 the simulation results for the n-ELAD (a) and p-ELAD (b) sensors with different readout implant sizes are shown. The simulated readout implant sizes are $20 \mu\text{m}$, $26 \mu\text{m}$, $30 \mu\text{m}$ and $40 \mu\text{m}$. The deep implant concentration in the n-ELAD and p-ELAD sensors is $3 \cdot 10^{15} \text{ cm}^{-3}$ and the biased voltage is 275 V and 300 V respectively. The black solid line in Fig. 7 denotes the $20 \mu\text{m}$ readout implant size option for both n-ELAD and

p-ELAD sensors, which was used for the simulations presented above. The black dash line shows the n-ELAD and p-ELAD sensors with the zero deep implant concentration and readout implant size of $20\text{ }\mu\text{m}$, which corresponds to the sensors with an epitaxial layer without deep implants. For the n-ELAD as well as for the p-ELAD sensors the size of the readout implant greatly changes the linearity of the η -function. The blue line in Fig. 7 (a) and (b) corresponds to the larger readout implant size of $40\text{ }\mu\text{m}$, the charge sharing effect in this option is weakest, it follows that with increasing of the readout implant the effect of the charge sharing decreases. Thus, the size of the readout cell is another parameter for tuning the shape of the η -function with different deep implants concentrations.

4 ELAD production technique

The realisation of the ELAD sensors requires a new production process combining several repetitive steps. Each step includes an ion beam surface implantation and epitaxial growth using the CVD³ method.

The first step of production is a surface ion implantation of the first layer of deep implants on a silicon wafer. On the top of the implanted silicon, an epitaxial layer is grown. The process is repeated three times. Finally, after the last epitaxial growth, common processes used for standard planar sensors are applied e.g. edging and preparation of readout implants.

As the CVD process imposes a large temperature budget on the implants, the process simulations have been executed in order to quantify a possible effect on the ELAD sensors performance. The results of the process simulations on a deep Boron implant after three 20 min temperature cycles show a change in the size of the deep implant in a range less than $1\text{ }\mu\text{m}$. The electric field and transient simulations have been validated according to this change in size, and show no effect on the η -function performance.

5 Conclusions

Development of the ELAD sensor is a new technologically-challenging project in silicon vertex sensors for high energy physics. In the ELAD sensors, active charge sharing is used in order to improve the position resolution without using a magnetic field or sensor tilt. The charge-sharing effect is achieved by changing the path of the charge carriers in the lateral direction in the bulk of the sensor. The well-tuned deep-implant structure creates a non-homogeneous electric field. Two types of sensors, n-ELAD and p-ELAD sensors, have been presented. The electric-field simulations for the 2D and 3D geometries show the electric field in the lateral direction created by the deep implants. The electric-field and transient simulations show the dependence of the η -function, and hence spatial resolution, in the ELAD sensors on the deep-implant concentration at a fixed pitch size. The TCAD simulations show a nearly linear η -function for $n_{di} = 2.4 \cdot 10^{15}\text{ cm}^{-3}$ at a bias voltage of $U=300\text{ V}$ for the p-ELAD sensor, demonstrating the possibility to obtain almost the theoretical optimum of charge sharing. The electric field profiles from 2D and 3D simulations will be used for Monte Carlo-based position resolution studies. Additionally, new manufacturing technique foreseen for the ELAD prototype production has been presented.

³Chemical Vapor Deposition

References

- [1] M. Aicheler, P. Burrows, M. Draper, T. Garvey, P. Lebrun, K. Peach, N. Phinney, H. Schmickler, D. Schulte, and N. Toge., “A multi-tev linear collider based on clic technology: Clic conceptual design report,” Geneva, 2012.
- [2] A. M. Nurnberg and D. Dannheim, “Requirements for the CLIC tracker readout,” Apr 2017. [Online]. Available: <https://cds.cern.ch/record/2261066>
- [3] S. Spannagel, “Test beam performance measurements for the phase i upgrade of the CMS pixel detector,” *Journal of Instrumentation*, vol. 12, no. 05, pp. P05 022–P05 022, may 2017. [Online]. Available: <https://doi.org/10.1088%2F1748-0221%2F12%2F05%2Fp05022>
- [4] G. L. Bayatian *et al.*, “CMS Physics: Technical Design Report Volume 1: Detector Performance and Software,” 2006. [Online]. Available: <https://cds.cern.ch/record/922757>
- [5] H. Jansen, “A pascalian lateral drift sensor,” *Nuclear Instruments and Methods in Physics Research Section A: Accelerators, Spectrometers, Detectors and Associated Equipment*, vol. 831, no. 1, pp. 242 – 245, 2016, proceedings of the 10th International “Hiroshima” Symposium on the Development and Application of Semiconductor Tracking Detectors. [Online]. Available: <http://www.sciencedirect.com/science/article/pii/S016890021600142X>
- [6] A. Velyka and H. Jansen, *Enhanced Lateral Drift Sensors: Concept and Development: Volume 2*. Springer, Singapore, 08 2018, pp. 380–384, proceedings of International Conference on Technology and Instrumentation in Particle Physics 2017.
- [7] “Synopsys web page,” <https://www.synopsys.com/>.
- [8] T. Poikela, J. Plosila, T. Westerlund, M. Campbell, M. D. Gaspari, X. Llopert, V. Gromov, R. Kluit, M. van Beuzekom, F. Zappone, V. Zivkovic, C. Brezina, K. Desch, Y. Fu, and A. Kruth, “Timepix3: a 65k channel hybrid pixel readout chip with simultaneous ToA/ToT and sparse readout,” *Journal of Instrumentation*, vol. 9, no. 05, pp. C05 013–C05 013, may 2014. [Online]. Available: <https://doi.org/10.1088%2F1748-0221%2F9%2F05%2Fc05013>